

Thermal Conductivity of sI CO₂ Clathrate Hydrate and the Effect of Guest Size in sI and sII Hydrates

Md Saiduzzaman, Paulo H. B Brant Carvalho, Nicolas Boulanger, Ulrich Häussermann, and Ove Andersson*



Cite This: *Energy Fuels* 2025, 39, 22574–22584



Read Online

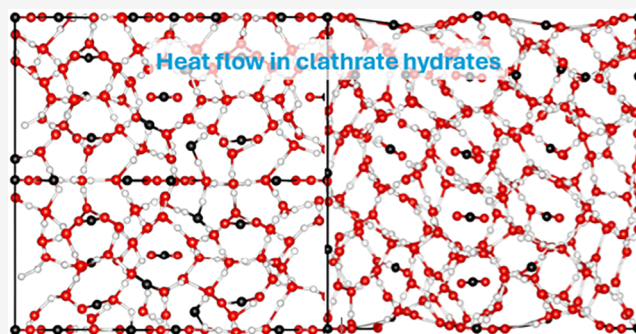
ACCESS |

 Metrics & More

 Article Recommendations

 Supporting Information

ABSTRACT: Clathrate hydrates are crystalline compounds in which guest molecules are encaged within an ice-like lattice. They occur naturally and possess properties of significant interest for energy and storage applications. Here, we report the thermal conductivity κ of structure I CO₂ clathrate hydrate across a broad temperature range (90–265 K) and at pressures up to 1.2 GPa. Similar to structure II clathrate hydrates, κ decreases with decreasing temperature, displaying almost identical temperature dependence. However, the absolute values are 10–30% lower. Notably, κ of CO₂ clathrate hydrate is among the lowest observed for structure I clathrate hydrates, with $\kappa = (426 \pm 8) \text{ mW m}^{-1} \text{ K}^{-1}$ under stable conditions at 270 K and 1 MPa. Furthermore, the isothermal dependencies of κ on density ρ and pressure p —parameters crucial for thermal modeling at elevated pressures—are relatively weak, with $(d \ln \kappa / d \ln \rho) = 1.2 \pm 0.2$ and $(d \ln \kappa / dp) = (12 \pm 1) \% \text{ GPa}^{-1}$. The measurements show significantly lower κ values and a different temperature dependence compared with previously reported simulation results. Nevertheless, the experimental data confirm the simulation prediction that κ for CO₂ clathrate hydrate is significantly lower than for other structure I clathrates. Our findings further indicate that κ in both structures I and II clathrate hydrates tends to decrease with increasing van der Waals radius of the guest molecules, as reviewed here. This trend may arise from enhanced distortion and anharmonicity within the ice framework. We tentatively propose that the pronounced anharmonicity of the clathrate hydrate lattice leads to frequent phonon–phonon scattering, effectively suppressing phonon-mediated heat transport and resulting in predominantly diffusive thermal conduction.



1. INTRODUCTION

A detailed understanding and knowledge of properties of naturally occurring clathrate hydrates (CHs) is essential for predicting and mitigating environmental changes on Earth. Global warming can lead to the decomposition of CHs trapped in permafrost and deep-sea sediments, resulting in the release of previously sequestered methane. Conversely, efforts in carbon capture and storage within controlled deep-sea environments may promote the formation of CHs, offering a more stable medium for carbon sequestration compared to gaseous or liquid forms.

The analysis of these processes depends heavily on key properties of CHs, particularly their stability and thermal characteristics. Notably, there is a significant gap in our knowledge of the thermal conductivity and heat capacity of carbon dioxide CH—a form that plays a crucial role not only in carbon storage strategies but also in planetary science.

CHs are inclusion compounds of water that can accommodate atoms or small molecules as guests. This characteristic makes CHs potential candidates for the solid-state storage of gases such as methane, hydrogen, and carbon dioxide. Some CHs naturally form under elevated pressures and low

temperatures and likely exist in substantial quantities on Earth and other celestial bodies. Therefore, the properties of CHs are important and have been extensively investigated. One notable discovery is the amorphous-like thermal conductivity of several CHs. Despite their crystalline structure, these CHs display a low magnitude and nearly temperature-independent thermal conductivity.¹ This atypical behavior for crystalline phases has been observed for both structure I (sI) CHs with guest molecules ethylene oxide,² xenon,^{3,4} methane,^{5–9} structure II (sII) CHs with guest molecules tetrahydrofuran,^{1,2,10–12} 1,3-dioxolane,¹³ cyclobutanone,¹³ cyclopentane,¹⁴ and structure H (sH) CH with guest methane–methylcyclohexane.¹⁵ The behavior is both of practical and academic significance; for instance, in the search for better thermoelectric materials, which require materials with low

Received: August 6, 2025

Revised: October 13, 2025

Accepted: November 10, 2025

Published: November 18, 2025



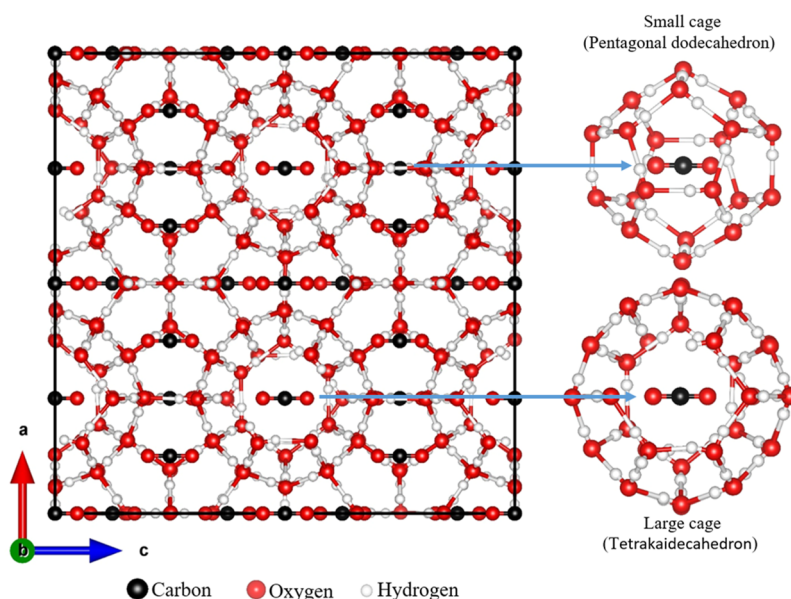


Figure 1. Structure of the sI CO_2 clathrate hydrate. Structural studies suggest that the large cages are filled and that the small cages are partially filled.

thermal conductivity but high electrical conductivity, and to gain better understanding of phonon propagation in complex crystals. However, the thermal conductivity of the important clathrate of carbon dioxide has not been studied in a wide temperature range and with a method that ensures a nonporous and ice-free sample. Such a method is crucial for accurate measurements of the magnitude and temperature behavior of the thermal conductivity.

At moderate pressures, carbon dioxide (CO_2) forms an sI CH where the unit cell contains 46 water molecules (Figure 1).^{16,17} The water molecules arrange themselves into a structure with six large tetraikaidcahedral cages and two small pentagonal dodecahedral cages per unit cell. This yields a composition of $\text{CO}_2 \cdot 5.75 \text{H}_2\text{O}$ when each cage is occupied by one CO_2 molecule. In an X-ray diffraction study of a single crystal of a CO_2 CH grown from deuterated water and liquid CO_2 at 276 K and 4 MPa, Udachin et al.¹⁸ found full occupancy of the large cages but that the small cages were only partly filled, about 71%, yielding a composition $\text{CO}_2 \cdot 6.20(15) \text{D}_2\text{O}$. However, the estimated compositions vary between studies, which can be partly explained by different synthesis conditions with higher occupancy for CO_2 CH formed at higher pressures.^{19,20}

Here, we have investigated the thermal conductivity of nonporous and ice-free sI CO_2 CH under pressure with the aim of understanding how guest species, density, temperature and pressure influence heat transport in sI CO_2 CH.

2. EXPERIMENTAL SECTION

2.1. Sample Preparation. The CO_2 CH samples were produced by similar procedures to those reported by Tulk et al.²¹ and Ikeda et al.²⁰ Powdered hexagonal ice was produced by freezing water (Sigma Ultrapur) and subsequently grinding it with a mortar and pestle in a cold atmosphere of boiling liquid nitrogen. The ice powder was then sieved/ground through a sieve (Sigma-Aldrich, ATM 100SS8F, Fine test sieve, 150 μm) with a stainless-steel frame, which was cooled by dry ice. The ice powder was collected in a Petri dish cooled by liquid nitrogen and subsequently transferred to a plastic bottle with a small hole in the cap, then stored in liquid nitrogen. During the sieving process, which took several hours, some water vapor condensed in the

Petri dish. Therefore, the material was sieved a second time, but this time with both the glass dewar and the fine test sieve cooled by dry ice. (The second sieving process was completed in 15 min.) A total of ca. 7 g of ice was produced and transferred to a pressure cylinder of 300 cm^3 capacity (Swagelok 304L Stainless Steel Double Ended DOT-Compliant Sample Cylinder), which was kept in dry ice during the transfer process. The sample cylinder was thereafter mounted in a setup equipped with a pressure gauge and two valves. One valve connected the cylinder to a CO_2 gas tube (Air Liquide, ≥ 99.9 vol % with water as the main impurity), and the other was initially connected to a vacuum pump. After filling with the ice powder, the sample cylinder was purged four times with CO_2 and then transferred to a freezer. The freezer maintained the cylinder temperature between 258 and 253 K for 1–3 days; the temperature was monitored with a type K thermocouple firmly attached to the cylinder. In total, we studied three samples, which were produced using slightly different procedures.

Sample #1: The pressure was initially kept at 1 MPa by occasionally refilling the sample cylinder to stay in the stable pressure–temperature range of sI CO_2 CH.²² Subsequently, the pressure was increased to 1.5 MPa, and the temperature was cycled between 271 and 257 K for 4 days. In total, the sample was kept a few degrees below zero, a range of relatively rapid clathrate growth, for 30 h. Thereafter, the cylinder pressure and temperature stabilized at (1.5 ± 0.05) MPa and (271 ± 0.5) K via a heating band around the sample vessel. The vessel and heater were thermally isolated from the freezer by a layer of glass fiber. Under these pressure–temperature conditions, the sample is kept 3–4 K below the stability limit of CO_2 CH. It remained under these conditions for 10 days before being recovered into a plastic bottle cooled by liquid nitrogen. The bottle was subsequently stored for 1 day in an absorption-based dewar at near-liquid nitrogen temperature before the sample was used to fill the thermal conductivity sample cell. Figure S1 shows the results for the thermal conductivity of sample #1 on heating at 0.06 GPa. The results are typical for a CH, i.e., weakly increasing on heating, but the results also show a transition near the CO_2 solid-to-liquid transition, which suggests that the sample contained a significant amount of solid CO_2 mixed with the CO_2 CH. The wire probe subsequently broke due to a power failure, which caused a pressure drop.

Sample #2: The pressure cylinder with powdered ice and pressurized CO_2 was initially kept at 0.6 MPa. Thereafter, the CO_2 pressure was raised gradually to 1.5 MPa while the temperature was increased to (271 ± 0.2) K. The temperature was maintained constant

for 33 days. The pressure cylinder was thereafter opened while kept at temperatures around 190 K. It was then heated to 208 K to remove solid CO₂; it remained above the CO₂ sublimation temperature (195 K) for 1.3 h before the sample was recovered in a plastic bottle and stored near liquid nitrogen temperature. This procedure yielded an almost pure CO₂ CH with only a slight excess of CO₂ (less than 1 vol %) as verified by X-ray powder diffraction (XRD) and thermal conductivity results (see Supporting Information).

Sample #3: The procedure to produce sample #3 was similar to that for sample #2. Based on the results for samples #1 and #2, we concluded that 15 days at 1.5 MPa and 271 K should be sufficient to produce a good CO₂ CH without a significant amount of ice. Since the results for sample #2 suggested a slight excess of solid CO₂ despite the treatment above the sublimation temperature, sample #3 was kept near 208 K for about 3 h to remove solid CO₂. However, after this treatment, the thermal conductivity results showed that the sample contained a significant amount of ice. The reason for the significant ice content is not certain, but it may have been caused by the longer annealing time near 208 K, even though the clathrate should be stable under these conditions. The results for sample #3 are shown in Figures S1 and S2.

2.2. X-ray Powder Diffraction Measurements. XRD measurements were performed using a PANalytical X'Pert³ Powder diffractometer equipped with Cu K α radiation ($\lambda = 1.5418 \text{ \AA}$). To enable low-temperature data collection, a TTK 600 low-temperature chamber (Anton Paar) was employed. The sample was cold-loaded into the precooled chamber at 150 K. Data were collected using a position-sensitive detector over the 2θ range of 10° to 65° , with a goniometer scan speed of $0.03^\circ \text{ s}^{-1}$ and data recorded at 0.013° intervals. Due to the detector's multichannel nature, each 0.013° step accumulated an equivalent total counting time of 118 s. Both empty sample holder and sample measurements showed signs of surface abrasion that introduced peaks from the sample holder in the diffraction patterns. These regions were excluded from the final fit, with little influence on the analysis.

2.3. Thermal Conductivity Measurements. The thermal conductivity was measured using the transient hot-wire method with a 42 mm long, 0.1 mm in diameter, Ni-wire as the hot-wire.^{23,24} The wire was mounted in a semicircular shape in a Teflon sample cell of 38 mm internal diameter. The temperature in the cell was measured by a calibrated Chromel versus Alumel thermocouple positioned close to the hot-wire. The cell was mounted on a bottom piston and inserted in a 45 mm internal diameter pressure cylinder of 1.3 GPa capacity. The sample was cold loaded into the cell at ca. 190 K by cooling the cylinder with liquid nitrogen while it was kept in a glovebag that had been purged several times with dry nitrogen gas. The space near the wire probe was filled with the sample while glass microspheres 0.2 mm in diameter were used to fill the remaining space in the cell. (Considering the low thermal diffusivity of the sample, the wire must be surrounded by ca. 1 mm of sample to avoid errors due to a limited sample size. In this case, the wire was surrounded by ca. 0.8 cm of sample.) The cell was closed with a Teflon lid, and a steel seal with indium coating and a hardened steel top piston were inserted in the cylinder. The whole assembly was transferred to a vacuum chamber and clamped to the precooled cold head of a closed He-cycle cryostat. To increase the temperature stability of the CH, the load was raised to ca. 0.07 GPa. The load was supplied by a fully automated hydraulic press. The pressure inside the cell was determined by measuring the signal from an oil pressure gauge, which had been previously calibrated to an accuracy of 0.05 GPa (at 1 GPa) in a separate experiment. This calibration was achieved by using the pressure-dependent resistance of a manganin wire.

The thermal conductivity was determined from the results of the wire temperature rise during a 1.4 s pulse of approximately constant power. Throughout the pulse, the resistance of the Ni-wire was measured over time (29 values), allowing for determination of the temperature increase. The equation for the temperature rise was fitted to the experimental data points, thereby yielding the thermal

conductivity with an uncertainty of $\pm 2\%$ (see Supporting Information and ref 23) and the heat capacity per unit volume ($\pm 5\%$).²³

3. RESULTS AND DISCUSSION

3.1. Sample Characterization. The production and characterization of the clathrate are crucial steps in reliably determining the thermal conductivity κ of CO₂ CH. In the case where each cage contains one CO₂ molecule, this is represented as CO₂·5.75H₂O. Since our sample was produced at 1.5 MPa and 271 K (1.5 times the equilibrium pressure for hydrate formation), we expect that it should initially have a composition close to that reported by Udachin et al.¹⁸ for a deuterated sample, i.e., CO₂·6.2 H₂O, which was formed at 2 times the equilibrium pressure for hydrate formation at 276 K. Because of the high κ of hexagonal ice, ice Ih,²⁴ it is particularly important to avoid excess ice in the sample. Although κ of CO₂ is also higher than that typically found for clathrates, it is only approximately 15% of κ of ice.²⁵ Thus, a slight excess of solid CO₂ affects κ less significantly than the same amount of excess ice.

To confirm that the sample was an sI CH, we conducted XRD analysis at 150 K (Figure 2). The results are consistent

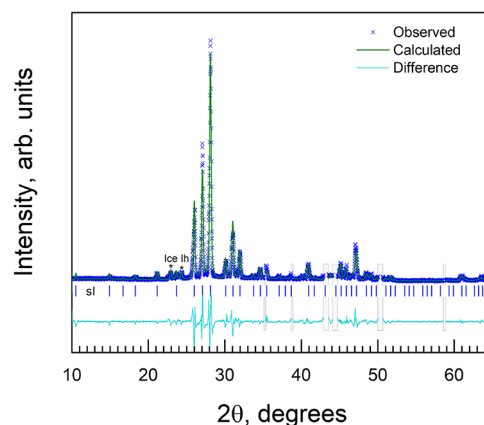


Figure 2. XRD of sample #2 at 150 K. The Le Bail refinement indicates that the sample is an sI clathrate hydrate (tick marks indicate Bragg reflection positions) with goodness of fit parameters $wR = 9.77\%$ and reduced $\chi^2 = 4.02$. The shaded regions were excluded from the refinement.

with the sI CH, characterized by a lattice parameter $a = 11.8767(3) \text{ \AA}$, $wR = 9.77\%$, reduced $\chi^2 = 4.02$. This is in good agreement with $a = 11.893(2) \text{ \AA}$ obtained from single crystal XRD for a deuterated sample at 173 K,¹⁸ $a = 11.872 \text{ \AA}$ reported from neutron powder diffraction data for a deuterated sample at 150 K,¹⁹ $a = 11.872 \text{ \AA}$ at 150 K,²⁶ and $a = 11.876 \text{ \AA}$ at 153 K²⁷ from powder XRD. The presence of ice Ih ($\sim 2 \text{ wt } \%$) was inferred from preliminary Rietveld analysis; however, the final Le Bail fit precludes quantitative phase estimation. The XRD pattern shows no detectable peaks corresponding to nonenclathrated CO₂. However, as discussed below, the κ measurements show that the sample was free of ice but that it contained a slight amount, less than 1 vol % (see Supporting Information), of nonenclathrated CO₂. We attribute this difference to the sample in the XRD study being loaded in a nondry atmosphere, which led to the condensation of humid air during the loading procedure and subsequent measurements.

3.2. Isobaric Thermal Conductivity. Figure 3 shows κ plotted against temperature for sample #2. All results reported

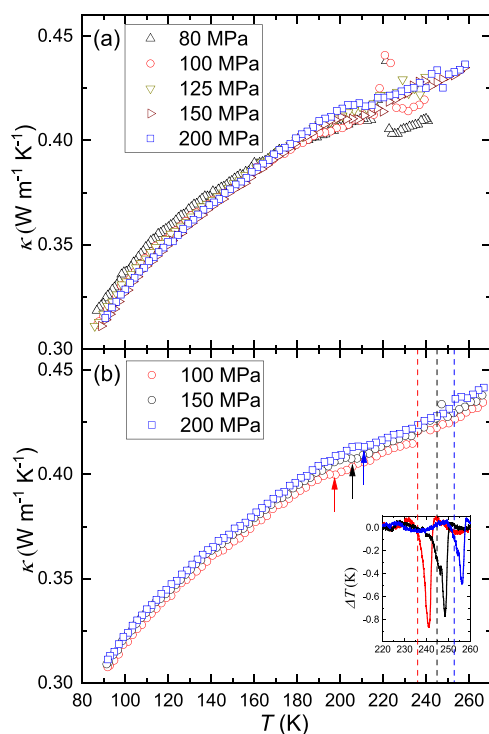


Figure 3. Thermal conductivity measured on cooling at pressures indicated: (a) prior to pressurization up to 1.2 GPa, and (b) after pressure cycling to 1.2 GPa at 130 K. The inset shows results derived from temperature versus time after subtraction of a polynomial function fitted to the data (below the transition). The dips are due to the solid-to-liquid CO_2 transition and show that the sample contained a slight amount of nonenclathrated CO_2 ; the vertical dashed lines indicate literature data for the solid-to-liquid CO_2 transition.³⁰ The vertical arrows indicate changes in $d\kappa/dT$, which are discussed in the text.

here pertain to this sample. (See Supporting Information for the results and analysis of samples #1 and #3.) Initially, the sample was temperature-cycled multiple times at gradually increasing pressures, as shown in Figure 3a. The results of weakly increasing κ on heating agree with the typical behavior reported for several sI and sII CHs. Moreover, a transition is observed as an anomalous, nonreal, peak in κ . This peak is caused by the heat of transformation, which reduces the temperature rise of the hot-wire probe. Above the transition, κ is slightly lower than below the transition. As discussed further below, the behavior is caused by a transition from solid CO_2 to liquid CO_2 , i.e., it shows that the sample contained nonenclathrated CO_2 . The transition features diminish as the sample is compressed and at the highest pressure, 200 MPa, the anomalous peak in κ can be observed but κ is almost the same at temperatures above the peak as it is below the peak. The slight change in behavior can be attributed to the effect of pressure. The initial state of the sample upon pressurization is porous, but the porosity decreases with pressurization, and homogeneity improves. Furthermore, the apparent slight excess of CO_2 may gradually fill the empty cages in the CO_2 CH upon repeated cycling above the transition at increasing pressure. The latter provides a plausible explanation for the slightly lower κ at 200 MPa compared to at 80 MPa at

temperatures below 180 K. The thermal conductivity of solid CO_2 increases upon cooling (Figure S1),²⁵ whereas that for CO_2 CH decreases. A decrease in excess solid CO_2 would therefore cause a reduction of κ of the sample. The slight change in κ , together with the diminishing transition features, suggests that excess CO_2 fills empty cages upon temperature cycling at high pressure.

Figure 3b shows results after the sample had been pressure-cycled to 1.2 GPa at 130 K. In studies of cellulose using the same experimental setup,^{28,29} it was shown that porous cellulose samples attain an essentially nonporous state at a pressure slightly below 0.5 GPa, which was inferred from the density and κ variation with pressure. Thus, the pressure cycling of CO_2 CH up to 1.2 GPa helps ensure that the sample is well compacted and in a nonporous state after the treatment.

The results in the range 0.1–0.2 GPa agree well and show that κ increases only weakly with pressure (Figure 3b), which is a typical result for CHs. Moreover, the slight decrease in κ at the solid-to-liquid CO_2 transition, observed in the uncompact sample, is difficult to detect in the well-compacted sample (see Figure S3). (The transition can be detected in the temperature data and agree well with literature data³⁰—see inset in Figure 3) This shows that the small amount of nonenclathrated CO_2 hardly affects κ of the sample outside the transition range. The results at 0.2 MPa agree within 1.5% with those measured before the high-pressure cycle up to 1.2 GPa. This suggests that the sample porosity, homogeneity and the cage occupation in the CO_2 CH did not change significantly after the first temperature cycle at 0.2 MPa. However, in addition to the solid–liquid transition of nonenclathrated CO_2 , the results show changes in $d\kappa/dT$ that occur at gradually higher temperatures with increasing pressure, as indicated by the vertical arrows in Figure 3b. These changes are weak, but since they were repeatable upon temperature cycling³¹ they may indicate a change in the sample. A previous study³¹ has also shown that the lattice parameter of CO_2 CH increases slightly at about 210 K upon cooling at 0.2 GPa. This unusual feature was attributed to an increase in the occupation number of CO_2 via double occupancy of some cages. It is therefore plausible that the changes in $d\kappa/dT$ (κ stays constant in a 6 K range) upon cooling are due to this effect. The structural study by Hirai et al.³¹ shows that the sI structure remains stable down to low temperatures despite the increase in the number of enclathrated CO_2 molecules.

The function $\ln \kappa = A - B/T$, where A and B are fitting parameters, provides a good description for κ of sII CHs.^{13,14} It also fits the results for CO_2 CH within 1.5%. However, to avoid a slight increase in uncertainty ($\pm 2\%$) associated with using this model function, we have employed a different function

$$\ln \kappa = \sum_{i=0}^2 A_i (\ln T)^i \quad (1)$$

where A_i are the fitted parameters, with the corresponding results provided in Table 1. This function describes the measured data to within 0.5% over the 90–265 K range, except in regions influenced by the CO_2 solid–liquid transition and the changes in $d\kappa/dT$ near 210 K.

3.3. Isothermal Thermal Conductivity. The stability of CO_2 CH was investigated through isothermal pressurization at 130 K (Figure 4) and 240 K (Figure 5). At 130 K, there is only a weak increase in κ that gradually levels off on pressurization.

Table 1. Fitting Functions of the Form: $\ln \kappa = \sum_{i=0}^2 A_i (\ln T)^i$, Which Describe the Measured κ Values to Within 0.5% over the 90–265 K Range^a

P (MPa)	A_0	A_1	A_2
0.1	-4.7317	1.1600	-0.0835
100	-4.8170	1.2000	-0.0874
150	-4.8585	1.2195	-0.0893
200	-4.8194	1.2028	-0.0873

^aAll values are in SI-units unless otherwise stated. The values at 0.1 MPa were calculated from the results at 0.10 GPa using the pressure dependence of κ between 0.10 and 0.15 GPa.

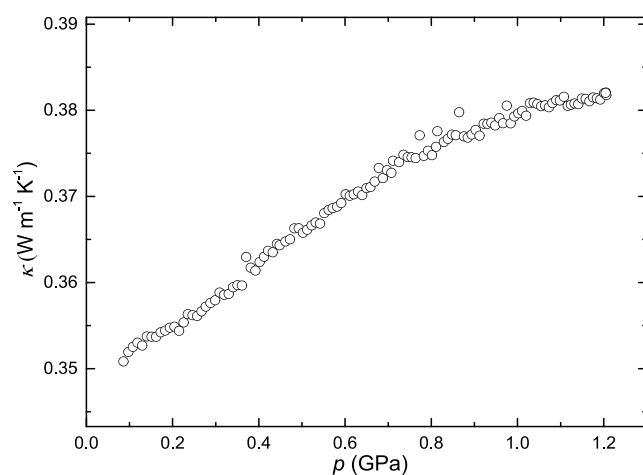


Figure 4. Thermal conductivity measured during pressure increase at 130 K.

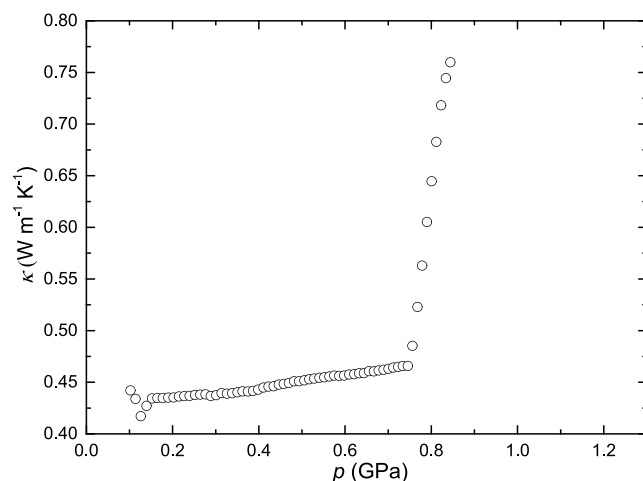


Figure 5. Thermal conductivity measured during pressure increase at 240 K.

This behavior is typical for materials not undergoing a transition. The leveling off mimics the behavior of the compressibility, indicating that the change in κ is closely associated with the densification of the CH. The behavior is strikingly different from that of sII CHs, which undergo pressure-induced amorphization (PIA) upon pressurization at 130 K.³² PIA of sII CHs manifests as a slight decrease in κ near 0.9 GPa due to crystalline lattice distortion, followed by an abrupt increase resulting from lattice collapse and a concurrent significant density increase. Since this is not observed here, it demonstrates that crystalline CO₂ CH remains stable up to at

least 1.2 GPa at 130 K. Based on the stability of other sI CHs, CO₂ CH is expected to be stable up to 3 GPa at 100 K.^{33–35} (Partial substitution of H₂O with NH₄F can significantly decrease the collapse pressure).³⁶

The data in Figure 4 also show that the sample did not contain a detectable amount of ice. Ice undergoes PIA near 1 GPa at temperatures below 140 K. During this process, κ decreases significantly, because κ of the crystalline phase is about five times that of the amorphous state. The substantial reduction makes even small amounts of ice easily detectable. This effect of PIA was previously observed in a sample containing cyclopentane CH;¹⁴ the study demonstrated that κ exhibited clear signs of PIA with just 1 wt % ice present in the sample. The absence of any PIA-related features in our data shows that any ice in the sample did not affect κ beyond the measurement precision of approximately 0.2%.

The behavior during pressurization at 240 K differs from that at lower temperatures (Figure 5). Initially, κ increases slightly, but at 0.75 GPa, it increases sharply. This shows that sI CO₂ CH remains stable up to 0.75 GPa at 240 K where it decomposes. The behavior is consistent with findings from high-pressure studies by Hirai et al.³¹ and Tulk et al.²¹ In the neutron scattering study by Tulk et al.,²¹ sI CO₂ CH was reported to decompose at 0.77 GPa under isothermal pressurization at 240 K, forming CO₂ filled ice, ice VI and solid CO₂. The high κ of ice VI, $\kappa = 1.6 \text{ W m}^{-1} \text{ K}^{-1}$ at 0.75 GPa and 240 K,²⁴ is the reason for the sharp increase of κ when the sample decomposes. Because of the volume change, the probe wire broke, and the experiment terminated.

Based on the measured $\kappa(p)$ and the isothermal bulk modulus B_T , we can derive the density dependence of κ , commonly expressed by the Bridgman parameter $g = (d \ln \kappa / d \ln \rho)_T$. From $\kappa(p)$ at 240 K, we obtain $(d \ln \kappa / dp)_T = (0.12 \pm 0.01) \text{ GPa}^{-1}$ in the range 0.15–0.65 GPa. The bulk modulus has been measured for sI CH with various guest molecules, e.g., CH₄,^{37–41} Xe,⁴² and C₂H₆,⁴² but not CO₂. In the latter case, only results of molecular dynamics simulations are available.^{43,44} To estimate the bulk modulus of CO₂ CH, we use the experimental data for the adiabatic bulk modulus B_S of CH₄CH measured by Helgerud et al.³⁸ and Shimizu et al.,³⁷ which agree within a few percent at pressures below 0.1 GPa, together with the isothermal results of Klapproth et al.³⁹ and simulation results.^{43,44} Based on these data, we calculate $B_T = (10.0 \pm 1.0) \text{ GPa}$ for CO₂ CH at 0.4 GPa and 240 K (see Supporting Information). Combining this with our results for $\kappa(p)$, yields $g = 1.2 \pm 0.2$, which is a relatively low density dependence compared to most crystalline phases. However, this value is not exceptionally low, as some crystalline phases—such as ice Ih—exhibit even negative density dependencies.

3.4. Comparison with Previous Results for sI and sII Clathrate Hydrates. The thermal properties of CHs have been recently reviewed by Sun et al.⁴⁵ To our knowledge, the only experimental κ data for CO₂ CH were measured in the range 264–282 K at pressures of 1.5–3 MPa,⁴⁶ and at 268 K at 0.1 MPa.⁴⁷ One study reported $\kappa \sim 0.65 \text{ W m}^{-1} \text{ K}^{-1}$ up to 274 K, rising to $\kappa \sim 1.07 \text{ W m}^{-1} \text{ K}^{-1}$ near decomposition;⁴⁶ the other reported $\kappa = 0.53 \text{ W m}^{-1} \text{ K}^{-1}$ at 268 K.⁴⁷ In both cases, the CH sample was produced by dissolving CO₂ gas in water and cooling, but the phase purity (i.e., ice content) was not explicitly verified. Forming an ice-free CO₂ CH requires several days of annealing of micron-sized ice under CO₂ pressure.^{20,21} Since even minute ice content strongly increases κ , we believe

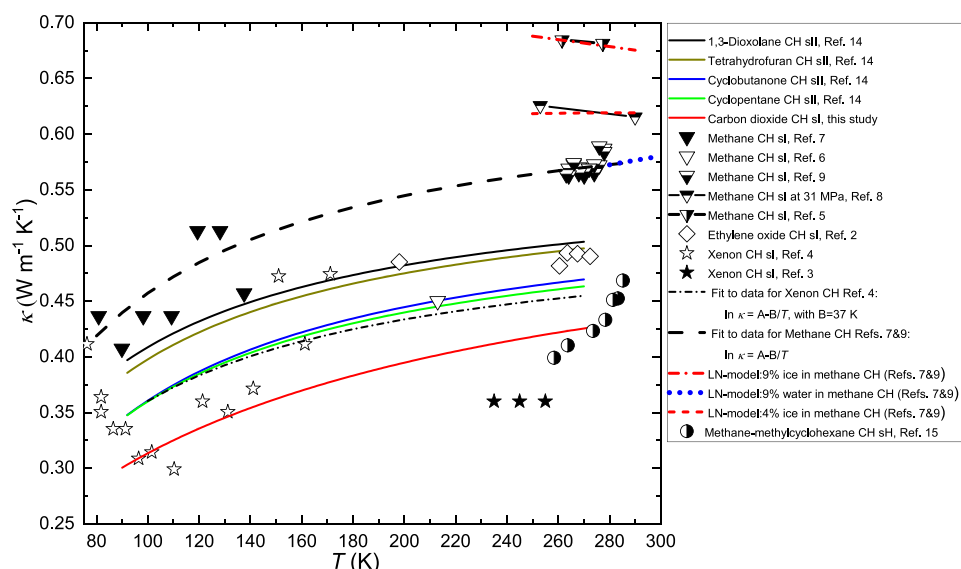


Figure 6. Thermal conductivity of clathrate hydrates as a function of temperature at or near atmospheric pressure unless otherwise stated. (A pressure increase of 30 MPa causes an increase in κ of only about 0.5%).⁸ The dash-dotted line representing κ of Xe CH is tentative due to the data scatter and that the fit of the data (above 110 K)⁴ assumed a similar temperature variation to other CHs, using an average B parameter of 37 K.

that the higher κ values found in these studies may be due to ice inclusions.

The thermal properties of CO_2 CH,⁴⁸ CH_4 CH, Xe CH and empty sI CHs, have also been explored in several simulations.^{5,48–51} In the range of our study, 90–260 K, the results suggest that κ of CO_2 CH decreases weakly with increasing temperature—a behavior typical of highly disordered crystals—and thus do not align with the experimental trends.

Before a comparison between the experimental results for sI, sII and sH CHs, it is instructive to discuss the effect of ice and porosity on the magnitude and temperature dependence of κ for CH samples. In a previous study,¹⁴ we showed that a mixture between an sII clathrate, tetrahydrofuran (THF) CH, and ice can be modeled with the Lewis-Nielsen (LN) model,⁵² which describes ice CH mixtures with high ice content well. The LN model is given by

$$\kappa_{\text{LN}} = \kappa_2 \left[\frac{1 + AB\phi}{1 - B\psi\phi} \right] \quad (2)$$

$$B = \frac{\frac{\kappa_1}{\kappa_2} - 1}{\frac{\kappa_1}{\kappa_2} + A} \quad (2b)$$

$$\psi = 1 + \left[\frac{1 - \phi_m}{\phi_m^2} \right] \phi \quad (2c)$$

where ϕ is the volume fraction of the component with thermal conductivity κ_1 (ice), and κ_2 is the thermal conductivity of the other component (CH); A and ϕ_m are two parameters in the LN model which depend on the shape and orientation of the dispersed phase (ice particles). For THF CH mixed with a relatively high concentration of ice, the values for randomly oriented rods with aspect ratio 15 and uniaxial random packing ($A = 8.38$ and $\phi_m = 0.82$),⁵² provided a good description.¹⁴ Using this model, we find that a sample with a typical CH (THF CH) and ice, shows crystal-like κ (i.e., decreasing κ) above 250 K when the ice content is about 5 vol % or higher.

Moreover, 5 vol % of ice increases the magnitude by 14% at 250 K, and significantly more at lower temperatures.

The studies of CH_4 CH by Rosenbaum et al.⁵ and White et al.⁸ illustrate well the importance of eliminating, or accounting for, the sample porosity ($= 1 - \rho_{\text{sample}}/\rho_{\text{nonporous sample}}$). Rosenbaum et al.⁵ showed that κ of their CH_4 CH sample increased from 0.15 to 0.68 $\text{W m}^{-1} \text{K}^{-1}$ during compression up to 45 MPa. White et al.⁸ estimated that the porosity of their synthesized material decreased from 34% to less than 5% by compression up to 104 MPa and holding for 4 days, but did not specify the change in κ . (In this study, we used 10 times higher pressure to eliminate the porosity of our synthesized sample.)

To compare the results for CO_2 CH with literature results of sI, sII and sH CH, we have compiled these in Figure 6. For guest material that dissolve in water, it is relatively easy to avoid ice and high porosity. These are the main causes of large errors because of the high κ of ice and low effective κ of a porous sample. Gas clathrate samples, however, can be difficult to obtain in a single clathrate phase. In these cases, one must carefully characterize the sample, or otherwise assess the effect of ice, but also consider the porosity to certify that the measured values are relevant as a measure of κ for the clathrate.

The compilation shown in Figure 6 suggests that κ of CO_2 CH is the lowest among all CHs in the 100–200 K range. The results for Xe CH near 250 K are lower, but if one considers the effect of temperature, these are not consistent with the Xe CH results measured at low temperatures. In the low-temperature study of Xe CH by Krivchikov et al.,⁴ the porosity issue was mitigated by introducing He gas to improve the thermal contact between clathrate grains, and they used a model to calculate κ of nonporous Xe CH. Extrapolating their data to higher temperatures suggests a higher κ than what was measured in the Xe clathrate study at 250 K.³ In the latter study, porosity was reduced by compacting the sample at 100 MPa, which is typically sufficient to achieve a nearly nonporous sample. However, because the measurements were conducted at pressures just above the dissociation pressure, the relaxation

upon pressure decrease likely led to a slight increase in porosity.

Most of the available data for sI, sII, and sH CHs indicate that their κ exhibits amorphous-like—or glass-like—behavior, characterized by a weak increase in κ with rising temperature. However, a few studies, particularly on CH₄ CHs, report the opposite trend, i.e., κ increasing with decreasing temperature. While the results for CH₄ CH generally show low κ values with weak temperature dependence, the specific behaviors vary across studies. These discrepancies may be attributed to differences in sample porosity and residual ice content. High porosity tends to lower κ and produce an amorphous-like temperature dependence, whereas significant ice content increases κ and leads to more crystal-like behavior.

There are four studies of CH₄ CHs that cover limited temperature ranges. Two of them show relatively high κ values with a negative temperature dependence,^{5,8} while the other two exhibit lower values with a positive temperature dependence (Figure 6).^{7,9} The latter results reported by Krivchikov et al.⁷ above 70 K and those of Huang and Fan⁹ appear to align well with the empirical correlation, $\ln \kappa = A - B/T$ with $A = -0.433$ and $B = 35.0$ K (dashed line in Figure 6), even though Huang and Fan⁹ did not apply high pressures to eliminate porosity. Moreover, if we combine this empirical correlation with the LN model, then the magnitude of the two other studies can be reproduced with 4 and 9 vol % ice, respectively (short-dashed lines in Figure 6). For one of the studies, the temperature dependence is also well reproduced. However, a good argument against this explanation is that any ice present in the sample should melt near 273 K, which would result in a step decrease in κ because of water's lower κ . The LN model with 9 vol % water instead of ice yields the dotted blue line in Figure 6, indicating that κ would decrease by $0.11 \text{ W m}^{-1} \text{ K}^{-1}$ when 9 vol % ice melts. But the results reported in refs 5 and 8 show no evidence of such a decrease. Adding to the complexity, some studies suggest that ice can persist in a metastable state within clathrates under pressure, even above its melting point—for example, at 290 K and 30 MPa.⁵³ Since none of the existing studies appear to be clearly erroneous, further investigation is needed to determine whether CH₄ CHs exhibit amorphous-like κ behavior, as observed in many other CHs, or if they represent an exception. Clarifying this behavior would also help reduce the uncertainty in κ values for CH₄ CH, which currently range from 0.56 to $0.68 \text{ W m}^{-1} \text{ K}^{-1}$ at temperatures above 250 K and pressures up to 100 MPa.

3.5. Correlations and Models for the Thermal Conductivity in Clathrate Hydrates. To provide a broad overview of κ of CHs, we summarize experimental and theoretical findings, excluding data potentially compromised by uncertain ice content or porosity. Figure 6 shows that κ of sII CHs decreases with the guest molecule in the sequence: 1,3-dioxolane (DXL, 2.8 Å), tetrahydrofuran (THF, 2.95 Å), cyclobutanone (CB, 3.25 Å), cyclopentane (CP, 3.05 Å), with the van der Waals radius of each molecule given in parentheses. As noted by Andersson and Ross,¹³ κ of the first three clathrates follow a decreasing trend with increasing molecular size. Figure 7 presents a plot of κ at 260 K as a function of the guest radius. The CP CH deviates slightly from the general trend observed. Notably, CP is the only guest in this sII series that lacks the ability to form even weak hydrogen bonds with the ice host lattice.

For sI CHs, κ decreases in the sequence: CH₄ (2.05 Å), ethylene oxide (EtO, 2.6 Å), Xe (2.2 Å), CO₂ (2.35 Å). Similar

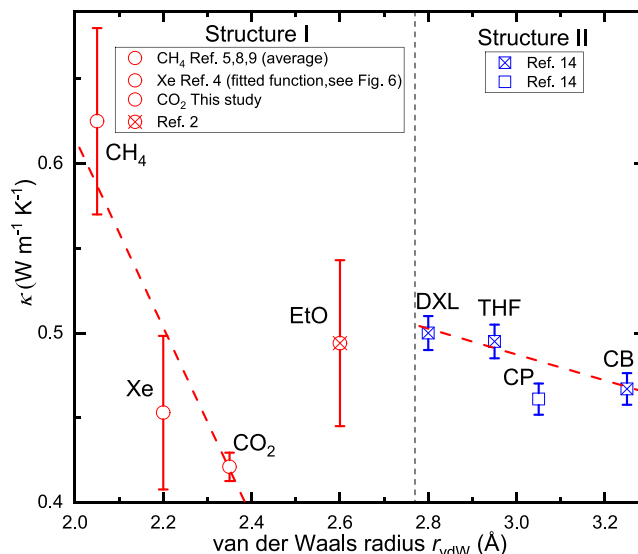


Figure 7. Thermal conductivity at 260 K plotted against the van der Waals radius r_{vdW} for guest molecules. The lines indicate the decreasing trend of κ with increasing guest size, with one significant exception for sI (ethylene oxide, EtO), and one slight exception for sII (cyclopentane, CP). Guest molecules with the possibility of forming hydrogen bonds with H₂O are indicated by a symbol with cross. The dashed red lines represent fits: $\kappa = 1.73(49) - 0.56(21) r_{vdW}$ for sI (excluding EtO) and $\kappa = 0.716(45) - 0.076(15) r_{vdW}$ for sII (excluding CP). The estimated measurement uncertainties (error bars) were used as weights ($= 1/\text{uncertainty}^2$) in the fits, and the uncertainties in the fitted parameters are the standard errors. (For CH₄ CH, we used an average of the reported values of refs 5,8,9 and half the range of the reported values for the estimated uncertainty.)

to the sII case, κ generally appears to decrease with increasing van der Waals size of the guest, with one notable exception: ethylene oxide, which can form hydrogen bonds. For sI hydrates, the decreasing trend among CHs with non-hydrogen bonded guests is less certain, attributable to uncertainties in the κ values for CH₄ and Xe CHs. A fit excluding the EtO value shows a decrease; however, the resulting slope has significant uncertainty (see caption of Figure 7). A tentative interpretation of these findings is that κ of both sI and sII generally decreases with increasing guest molecule size, but that guest–host interactions via hydrogen bonds slightly promote heat transfer compared to CHs with guests of similar size that cannot form hydrogen bonds.

Regarding simulations, the study by Jiang and Jordan⁴⁸ effectively reproduces the observed trend for sI CHs. They compared the impact of encaging CO₂, Xe and CH₄ in CHs. Although their simulations do not quantitatively match experimental values, they suggest that κ of CO₂ CH is approximately 25% lower than that of CH₄ CH at 260 K in good agreement with experimental data. This reduction was attributed to stronger guest–host coupling, even though they found it less important at high temperatures. In the present study, the measured κ values of CO₂ CH are 25–38% lower than those reported for CH₄ CHs.^{5,8,9} Furthermore, the simulation results of Jiang and Jordan⁴⁸ are also consistent with the slightly higher κ for Xe clathrate compared to CO₂ clathrate, as reflected in our comparison with the data of Krivchikov et al. (Figure 6).⁴

A significant number of studies have attempted to unravel the origin of the amorphous-like behavior of κ in CHs. The

initial hypothesis—strong phonon scattering due to dynamic disorder in guest molecule orientations¹—was disproven when CHs with monatomic guests like xenon exhibited similar behavior.^{3,4} However, strong phonon scattering resulting from interactions between rattling guest atoms and the ice lattice,¹⁰ known as the resonant scattering model,⁵⁴ remains a viable explanation, despite negative evidence for this mechanism in other inclusion compounds.^{55,56} (In these compounds, alternative explanations such as strong Umklapp scattering⁵⁵ and flat phonon dispersion relations, i.e., near-zero phonon velocities,⁵⁶ have been proposed.)

An early theoretical analysis attributed the amorphous-like behavior to the large number of oxygen atoms per unit cell n in CHs.⁵⁷ These give rise to numerous optical modes, which can scatter propagating phonons but are assumed to contribute little to heat conduction. The core of this analysis is that frequent scattering leads to a mean free path inversely proportional to $n^{2/3}$, potentially reducing it to nearly the interatomic spacing. However, both the present study and previous investigations show that an sI CH with $n = 46$ oxygen atoms per unit cell can exhibit lower κ than sII CHs with $n = 136$ suggesting an even shorter mean free path in the former.

Several simulations have been conducted to examine the explanations for the low and amorphous-like κ observed in CHs. An early study by Inoue et al.⁵¹ supported the resonant scattering model and suggested that phonon scattering is primarily, though not exclusively, caused by the encaging of guest molecules. (However, a subsequent study reported that their results may have been influenced by incomplete convergence).⁴⁹ Later investigations have explored the behavior in greater detail, and the findings generally suggest that κ depends on both the structure of the hydrate and the nature of the guest molecule. In particular, empty CHs exhibit lower κ than ice, and this reduction is more significant than that resulting from guest molecule encaging. For instance, English et al.⁵⁰ found that the change of structure from ice Ih to empty sI caused equal or larger reduction in κ than the change from empty sI to sI with encaged CH₄. However, the amorphous-like κ , which they found at temperatures above 150 K, was attributed to guest–host interactions. In contrast, Jiang and Jordan⁴⁸ reported a smaller effect on κ due to CH₄ encaging in sI, with virtually no change above 100 K.

English et al.⁵⁰ ascribed the structure-related reduction in κ to a more distorted ice framework in CHs compared to ice Ih. They also discussed the different effect of CH₄ inclusion in sI and sII, emphasizing that in sII—where larger cages provide additional free space—a greater amplitude of thermal rattling is needed to bring about the intermittent close guest–host contact required for heat-transport dissipation. This interpretation is consistent with the observed guest-size-dependent effects on κ shown in Figure 7.

Based on the available results, the key mechanism responsible for the low and amorphous-like κ in CHs cannot be confidently identified. The difference compared to ice may arise from structural changes, guest–host interactions, or a combination of both. The transformation from Ih structure to sI, sII or sH increases the number of optical modes and the anharmonicity of the ice lattice due to distortion and the resulting changes of the potentials, and large and rattling guests may cause a further increase, as well as resonant scattering.

Concerning possible mechanisms for the low κ , we can quantitatively estimate the change of one key property in determining κ of a material—the lattice anharmonicity; it is

typically described by the mode Grüneisen parameters: $\gamma_i = (d \ln \nu_i)/(d \ln \rho)_T$, where ν_i is the vibrational frequency of mode i . In a simplified description, it can be described by an average for the modes most relevant for heat conduction, i.e., the acoustic (phonon) modes in well-ordered crystals and diffusive modes in amorphous materials. We have previously determined that the change from proton-disordered ice (ice Ih) to proton-ordered ice (ice XI) is well described by a reduction in the anharmonicity of the ice lattice.⁵⁸ The same type of transition in THF CH is also well described by an identical change in the anharmonicity, despite that κ is crystal-like in ice but amorphous-like in CHs.¹² To estimate the change in anharmonicity of the ice lattice due to the structural change, we consider the thermodynamic relation

$$\gamma_{\text{th}} = \frac{\alpha B_s}{C_p \rho} \quad (3)$$

where α is the volume thermal expansion coefficient and C_p is the isobaric specific heat. It has been calculated for THF CH by Tse,⁵⁹ while Fortes⁶⁰ and Leadbetter⁶¹ have conducted careful analyses for ice Ih. Their results are presented in Figure 8. If we consider γ_{th} at high temperatures, which gives the high

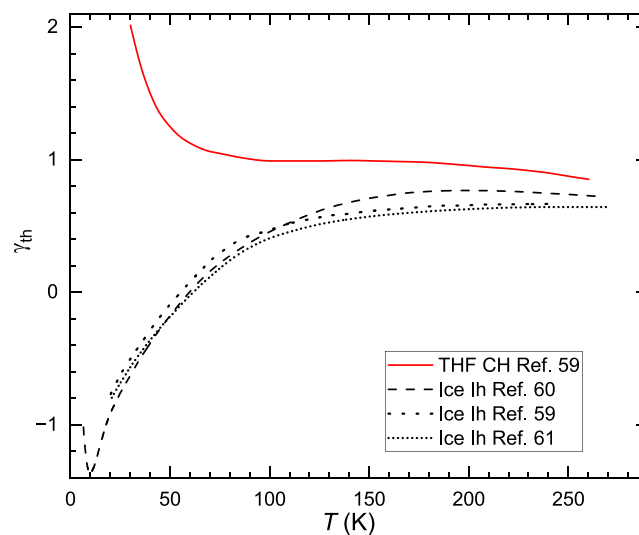


Figure 8. Thermodynamic Grüneisen parameter plotted against temperature for ice Ih,^{59–61} and THF CH.⁵⁹ Adapted from Tse⁵⁹ with permission. Copyright 1987 EDP Sciences.

temperature limiting value of γ_{th} and should be an average of γ for the modes that contribute significantly to the heat capacity, then γ_{th} differs by about 25% between ice and THF CH. The larger anharmonicity in clathrates has been noted and discussed previously,^{59,62} but perhaps not extensively in the context of significantly increased phonon–phonon scattering, which we investigate below.

It is important to note that a mechanism that increases phonon–phonon scattering cannot, by itself, explain a change from crystal-like to amorphous-like κ unless the scattering becomes sufficiently frequent to reduce the phonon mean free path to the scale of interatomic (oxygen–oxygen) distances. Concurrently, with increasing scattering, a gradual transformation from phonon-mediated (crystal-like) to diffusive (amorphous-like) heat transport is expected. Notably, the results of Krivchikov et al.⁴ indicate that such a transformation occurs around 100 K upon heating Xe and CH₄ CHs.

It is reasonable to assume that the phonon–phonon scattering rate varies strongly with γ , typically as γ^2 .⁶³ Moreover, κ of ice is approximately described by $\kappa = A \cdot T^{-1}$ where $A = 630 \text{ W m}^{-1}$.²⁴ With $A \propto \gamma^{-2}$, the 25% increase in γ_{th} would cause a decrease from $\kappa = 6.3$ to $4 \text{ W m}^{-1} \text{ K}^{-1}$ ($\Delta \ln \kappa = -2 \cdot \Delta \ln \gamma$) at 100 K. This is far from sufficient to explain the approximately 16-fold decrease in κ between ice and CHs at 100 K. However, if we focus on low-frequency phonons by instead evaluating γ_{th} at lower temperatures, e.g., at 70 K, where Leadbetter⁶¹ found that librations start to contribute significantly to the heat capacity, then the change in γ_{th} suggests a 38-fold decrease in κ , i.e., an even too large reduction of κ . But in this case the significantly increased scattering rate would limit the phonon mean free path to the order of the oxygen–oxygen spacing, and heat transport would change from phonon to diffusive heat transfer.

Experimental support for low-frequency phonons being the dominant heat-carrying modes in ice is found in results for the pressure dependence of κ for ice Ih, which is negative.²⁴ In contrast, κ of CHs increases weakly on pressurization (Figures 4 and 5). The unusual result for ice is explained by a negative Grüneisen parameter,⁶³ which supports that the most representative (average) γ_{th} for evaluation of κ of ice is obtained from values below 70 K.

The above calculation suggests that the altered anharmonicity of the ice lattice, when transformed from ice Ih to a CH containing guest molecules, may explain the significant reduction of κ . This reduction would be due to significantly increased phonon–phonon scattering, involving both optical and acoustic phonons, which effectively quenches the heat carried by phonons and induces diffusive heat transfer. In this context, weak hydrogen bond guest–host interactions may facilitate heat transfer compared to non-hydrogen bonding guests, as indicated by the results in Figure 7. This model for the thermal resistivity in CHs aligns with the findings of Koza et al.⁵⁵ regarding the absence of freely “rattling” guests, and thus no resonant scattering by guest atoms in La- and Ce-filled $\text{Fe}_4\text{Sb}_{12}$ skutterudites. However, further experimental results, preferably for empty CHs, as well as comprehensive simulations (such as the studies by English et al.⁵⁰ and Jiang and Jordan⁴⁸ using improved models) are necessary to fully elucidate the mechanism underlying the amorphous-like behavior of κ in CHs.

4. CONCLUSIONS

The thermal conductivity of nonporous and ice-free sI CO_2 CH under stability conditions in the 90–270 K range is amorphous-like, with a magnitude of $\kappa = (426 \pm 8) \text{ mW m}^{-1} \text{ K}^{-1}$ at 270 K. It increases by only 1% for every percentage increase in density, or by 12% GPa^{-1} with pressure increase. The magnitude is among the lowest measured for CHs, irrespective of structure (sI, sII and sH). The thermal conductivity is 25–38% lower than that of CH_4 CH, which supports simulations showing a 25% decrease for a change of guest from CH_4 to CO_2 in sI.⁴⁸ The temperature dependence of κ is identical to that of sII CHs, suggesting that the phonon mean free paths in both sI and sII are about the size of the interoxygen spacing and that diffusive modes dominate heat transfer. The results here, together with literature results for both sI and sII CHs, suggest a correlation between guest size and κ , with κ decreasing weakly with increasing guest size, but also that guest–host hydrogen bond interactions promote κ .

A tentative explanation for the amorphous-like κ of CHs is that the high anharmonicity of the ice lattice causes frequent phonon–phonon scattering to such an extent that it essentially quenches heat transfer mediated by phonons. As a consequence, the heat transfer becomes diffusive and therefore amorphous-like, with only a weak dependence on the guest species.

■ ASSOCIATED CONTENT

Supporting Information

The Supporting Information is available free of charge at <https://pubs.acs.org/doi/10.1021/acs.energyfuels.5c04143>.

Thermal conductivity of samples #1 and #3, estimation of nonenclathrated CO_2 content in sample #2, estimation of the isothermal bulk modulus of CO_2 CH at 240 K and 0.4 GPa, contributions to the uncertainty in thermal conductivity (PDF)

■ AUTHOR INFORMATION

Corresponding Author

Ove Andersson – Department of Physics, Umeå University, 901 87 Umeå, Sweden; orcid.org/0000-0003-1748-9175; Email: ove.b.andersson@umu.se

Authors

Md Saiduzzaman – Department of Physics, Umeå University, 901 87 Umeå, Sweden; Department of Materials Science and Engineering, Khulna University of Engineering & Technology (KUET), Khulna 9203, Bangladesh

Paulo H. B Brant Carvalho – Department of Chemistry—Ångström Laboratory, Uppsala University, 751 21 Uppsala, Sweden

Nicolas Boulanger – Department of Physics, Umeå University, 901 87 Umeå, Sweden

Ulrich Häussermann – Department of Chemistry, Stockholm University, 106 91 Stockholm, Sweden; orcid.org/0000-0003-2001-4410

Complete contact information is available at: <https://pubs.acs.org/10.1021/acs.energyfuels.5c04143>

Notes

The authors declare no competing financial interest.

■ ACKNOWLEDGMENTS

We acknowledge financial support from Carl Tryggers Stiftelse (CTS 22:1980) and Stiftelsen Olle Engkvist Byggmästare (216-0468) (MS). P.H.B.B.C. acknowledges financial support from the SSF-SwedNESS grant SNP21-0002.

■ REFERENCES

- (1) Ross, R. G.; Andersson, P.; Bäckström, G. Unusual PT Dependence of the Thermal Conductivity for a Clathrate Hydrate. *Nature* **1981**, *290*, 322–323.
- (2) Cook, J. G.; Laubitz, M. J. *Thermal Conductivity*; Hust, J. G., Ed.; Plenum Press: New York, 1983; Vol. 17, pp 745–751.
- (3) Handa, Y. P.; Cook, J. G. Thermal Conductivity of Xenon Hydrate. *J. Phys. Chem. A* **1987**, *91*, 6327–6328.
- (4) Krivchikov, A. I.; Gorodilov, B. Y.; Korolyuk, O. A.; Manzhelii, V. G.; Romantsova, O. O.; Conrad, H.; Press, W.; Tse, J. S.; Klug, D. D. Thermal conductivity of Xe clathrate hydrate at low temperatures. *Phys. Rev. B* **2006**, *73*, No. 064203.
- (5) Rosenbaum, E. J.; English, N. J.; Johnson, J. K.; Shaw, D. W.; Warzinski, R. P. Thermal conductivity of methane hydrate from

- experiment and molecular simulation. *J. Phys. Chem. B* **2007**, *111*, 13194–13205.
- (6) Cook, J. G.; Leaist, D. G. An exploratory study of the thermal conductivity of methane hydrate. *Geophys. Res. Lett.* **1983**, *10*, 397–399.
- (7) Krivchikov, A. I.; Gorodilov, B. Ya.; Korolyuk, O.; Manzhelii, V. G.; Conrad, H.; Press, W. Thermal Conductivity of Methane-Hydrate. *J. Low Temp. Phys.* **2005**, *139*, 693–702.
- (8) Waite, W. F.; Stern, L. A.; Kirby, S. H.; Winters, W. J.; Mason, D. H. Simultaneous determination of thermal conductivity, thermal diffusivity and specific heat in sI methane hydrate. *Geophys. J. Int.* **2007**, *169*, 767–774.
- (9) Huang, D.; Fan, S. Thermal Conductivity of Methane Hydrate Formed from Sodium Dodecyl Sulfate Solution. *J. Chem. Eng. Data* **2004**, *49*, 1479–1482.
- (10) Krivchikov, A. I.; Manzhelii, V. G.; Korolyuk, O. A.; Gorodilov, B. Ya.; Romantsova, O. O. Thermal conductivity of tetrahydrofuran hydrate. *Phys. Chem. Chem. Phys.* **2005**, *7*, 728–730.
- (11) Ashworth, T.; Johnson, L. R.; Lai, L.-P. *Thermal Conductivity Of Pure Ice And Tetrahydrofuran Clathrate Hydrates*; European thermophysical properties conference; Pion, 1985; pp 413–419.
- (12) Andersson, O.; Suga, H. Thermal conductivity of normal and deuterated tetrahydrofuran clathrate hydrates. *J. Phys. Chem. Solids* **1996**, *57*, 125–132.
- (13) Andersson, P.; Ross, R. G. Effect of guest molecule size on the thermal conductivity and heat capacity of clathrate hydrates. *J. Phys. C: Solid State Phys.* **1983**, *16*, 1423–1432.
- (14) Andersson, O.; Saiduzzaman, M.; Carvalho, P. H. B. B.; Häussermann, U. Amorphous-like thermal conductivity and high mechanical stability of cyclopentane clathrate hydrate. *Phys. Chem. Chem. Phys.* **2024**, *26*, 16017–16025.
- (15) Li, D.; Liang, D.; Peng, H.; Wan, L. Thermal conductivities of methane-methylcyclohexane and tetrabutylammonium bromide clathrate hydrate. *J. Therm. Anal. Calorim.* **2016**, *123*, 1391–1397.
- (16) Davidson, D. W. In *Water: A Comprehensive Treatise*; Franks, F., Ed.; Plenum Press: New York, 1973; Vol. 2, pp 115–234.
- (17) Sloan, E. D.; Koh, C. A. *Clathrate Hydrates of Natural Gases*, 3rd ed.; CRC Press: Boca Raton, FL, 2007 DOI: 10.1201/9781420008494.
- (18) Udachin, K. A.; Ratcliffe, C. I.; Ripmeester, J. A. Structure, Composition, and Thermal Expansion of CO₂ Hydrate from Single Crystal X-ray Diffraction Measurements. *J. Phys. Chem. B* **2001**, *105*, 4200–4204.
- (19) Henning, R. W.; Schultz, A. J.; Thieu, V.; Halpern, Y. Neutron Diffraction Studies of CO₂ Clathrate Hydrate: Formation from Deuterated Ice. *J. Phys. Chem. A* **2000**, *104*, 5066–5071.
- (20) Ikeda, T.; Mae, S.; Yamamuro, O.; Matsuo, T.; Ikeda, S.; Ibberson, R. M. Distortion of Host Lattice in Clathrate Hydrate as a Function of Guest Molecule and Temperature. *J. Phys. Chem. A* **2000**, *104*, 10623–10630.
- (21) Tulk, C. A.; Machida, S.; Klug, D. D.; Lu, H.; Guthrie, M.; Molaison, J. J. The structure of CO₂ hydrate between 0.7 and 1.0 GPa. *J. Chem. Phys.* **2014**, *141*, No. 174503.
- (22) Wendland, M.; Hasse, H.; Maurer, G. Experimental Pressure-Temperature Data on Three- and Four-Phase Equilibria of Fluid, Hydrate, and Ice Phases in the System Carbon Dioxide–Water. *J. Chem. Eng. Data* **1999**, *44*, 901–906.
- (23) Håkansson, B.; Andersson, P.; Bäckström, G. Improved Hotwire Procedure for Thermophysical Measurements under Pressure. *Rev. Sci. Instrum.* **1988**, *59*, 2269–2275.
- (24) Andersson, O.; Inaba, A. Thermal Conductivity of Crystalline and Amorphous Ices and Its Implications on Amorphization and Glassy Water. *Phys. Chem. Chem. Phys.* **2005**, *7*, 1441–1449.
- (25) Saiduzzaman, M.; Konstantinov, V. A.; Andersson, O. Thermal Conductivity of Solid Carbon Dioxide. *Int. J. Thermophys.* **2025**, *46*, No. 70.
- (26) Hansen, T. C.; Falenty, A.; Kuhs, W. F. Lattice Constants and Expansivities of Gas Hydrates from 10 K up to the Stability Limit. *J. Chem. Phys.* **2016**, *144*, No. 054301.
- (27) Hester, K. C.; Huo, Z.; Ballard, A. L.; Koh, C. A.; Miller, K. T.; Sloan, E. D. Thermal Expansivity for sI and sII Clathrate Hydrates. *J. Phys. Chem. B* **2007**, *111*, 8830–8835.
- (28) Antlauf, M.; Boulanger, N.; Berglund, L.; Oksman, K.; Andersson, O. Thermal Conductivity of Cellulose Fibers in Different Size Scales and Densities. *Biomacromolecules* **2021**, *22*, 3800–3809.
- (29) Antlauf, M.; Andersson, O. Thermal Conductivity of Porous and Dense Networks of Cellulose Nanocrystals. *Macromolecules* **2022**, *55*, 5326–5331.
- (30) Span, R.; Wagner, W. A New Equation of State for Carbon Dioxide Covering the Fluid Region from the Triple-Point Temperature to 1100 K at Pressures up to 800 MPa. *J. Phys. Chem. Ref. Data* **1996**, *25*, 1509–1596.
- (31) Hirai, H.; Komatsu, K.; Honda, M.; Kawamura, T.; Yamamoto, Y.; Yagi, T. Phase Changes of CO₂ Hydrate under High Pressure and Low Temperature. *J. Chem. Phys.* **2010**, *133*, No. 124511.
- (32) Andersson, O.; Carvalho, P. H. B. B.; Hsu, Y.-J.; Häussermann, U. Transitions in pressure-amorphized clathrate hydrates akin to those of amorphous ices. *J. Chem. Phys.* **2019**, *151*, No. 014502.
- (33) Tulk, C. A.; Klug, D. D.; Molaison, J. J.; dos Santos, A. M.; Pradhan, N. Structure and stability of an amorphous water–methane mixture produced by cold compression of methane hydrate. *Phys. Rev. B* **2012**, *86*, No. 054110.
- (34) Carvalho, P. H. B. B.; Mace, A.; Andersson, O.; Tulk, C. A.; Molaison, J.; Lyubartsev, A. P.; Nangoi, I. M.; Leitão, A. A.; Häussermann, U. Pressure-induced amorphization of noble gas clathrate hydrates. *Phys. Rev. B* **2021**, *103*, No. 064205.
- (35) Noguchi, N.; Shiraishi, Y.; Kageyama, M.; Yokoi, Y.; Kurohama, S.; Okada, N.; Okamura, H. Direct observation of pressure-induced amorphization of methane/ethane hydrates using Raman and infrared spectroscopy. *Phys. Chem. Chem. Phys.* **2023**, *25*, 22161–22170.
- (36) Fidler, L.-R.; Posch, P.; Klocker, J.; Hofer, T. S.; Loerting, T. The impact of alcohol and ammonium fluoride on pressure-induced amorphization of cubic structure I clathrate hydrates. *J. Chem. Phys.* **2024**, *160*, No. 194504.
- (37) Shimizu, H.; Kumazaki, T.; Kume, T.; Sasaki, S. Elasticity of single-crystal methane hydrate at high pressure. *Phys. Rev. B* **2002**, *65*, No. 212102.
- (38) Helgerud, M. B.; Waite, W. F.; Kirby, S. H.; Nur, A. Elastic Wave Speeds and Moduli in Polycrystalline Ice Ih, sI Methane Hydrate, and sII Methane-Ethane Hydrate. *J. Geophys. Res.* **2009**, *114*, No. B02212.
- (39) Klapproth, A.; Goreschnik, E.; Staykova, D.; Klein, H.; Kuhs, W. F. Structural Studies of Gas Hydrates. *Can. J. Phys.* **2003**, *81*, 503–518.
- (40) Hirai, H.; Kondo, T.; Hasegawa, M.; Yagi, T.; Yamamoto, Y.; Komai, T.; Nagashima, K.; Sakashita, M.; Fujihisa, H.; Aoki, K. Methane Hydrate Behavior under High Pressure. *J. Phys. Chem. B* **2000**, *104*, 1429–1433.
- (41) Hirai, H.; Uchihara, Y.; Fujihisa, H.; Sakashita, M.; Katoh, E.; Aoki, K.; Nagashima, K.; Yamamoto, Y.; Yagi, T. High-pressure structures of methane hydrate observed up to 8 GPa at room temperature. *J. Chem. Phys.* **2001**, *115*, 7066–7070.
- (42) Manakov, A. Yu.; Likhacheva, A. Yu.; Potemkin, V. A.; Ogienko, A. G.; Kurnosov, A. V.; Ancharov, A. I. Compressibility of Gas Hydrates. *ChemPhysChem* **2011**, *12*, 2476–2484.
- (43) Ning, F. L.; Glavatskiy, K.; Ji, Z.; Kjelstrup, S.; Vlught, T. J. H. Compressibility, thermal expansion coefficient and heat capacity of CH₄ and CO₂ hydrate mixtures using molecular dynamics simulations. *Phys. Chem. Chem. Phys.* **2015**, *17*, 2869–2883.
- (44) Jia, J.; Liang, Y.; Tsuji, T.; Murata, S.; Matsuoka, T. Elasticity and Stability of Clathrate Hydrate: Role of Guest Molecule Motions. *Sci. Rep.* **2017**, *7*, No. 1290.
- (45) Sun, S.; Gu, L.; Yang, Z.; Lin, H.; Li, Y. Thermophysical Properties of Natural Gas Hydrates: A Review. *Nat. Gas Ind. B* **2022**, *9*, 246–263.
- (46) Wan, L.; Liang, D.; Li, D.; Guan, J. Characteristics of Thermal Conductivity and Thermal Diffusivity of Carbon Dioxide Hydrate. *CIESC J.* **2016**, *67*, 4169–4175.

(47) Jiao, L. J.; Wan, R. C.; Wang, Z. L. Experimental Investigation of CO₂ Hydrate Dissociation in Silica Nanoparticle System with Different Thermal Conductivity. *Int. J. Thermophys.* **2021**, *42*, No. 170.

(48) Jiang, H.; Jordan, K. D. Comparison of the Properties of Xenon, Methane, and Carbon Dioxide Hydrates from Equilibrium and Nonequilibrium Molecular Dynamics Simulations. *J. Phys. Chem. C* **2010**, *114*, 5555–5564.

(49) Jiang, H.; Myshakin, E. M.; Jordan, K. D.; Warzinski, R. P. Molecular Dynamics Simulations of the Thermal Conductivity of Methane Hydrate. *J. Phys. Chem. B* **2008**, *112*, 10207–10216.

(50) English, N. J.; Tse, J. S.; Carey, D. J. Mechanisms for Thermal Conduction in Various Polymorphs of Methane Hydrate. *Phys. Rev. B* **2009**, *80*, No. 134306.

(51) Inoue, R.; Tanaka, H.; Nakanishi, K. Molecular Dynamics Simulation Study of the Anomalous Thermal Conductivity of Clathrate Hydrates. *J. Chem. Phys.* **1996**, *104*, 9569–9577.

(52) Nielsen, L. E. The Thermal and Electrical Conductivity of Two-Phase Systems. *Ind. Eng. Chem. Fundam.* **1974**, *13*, 17–20.

(53) Stern, L. A.; Kirby, S. H.; Durham, W. B. Polycrystalline Methane Hydrate: Synthesis from Superheated Ice, and Low-Temperature Mechanical Properties. *Energy Fuels* **1998**, *12*, 201–211.

(54) Tse, J. S.; White, M. A. Origin of glassy crystalline behavior in the thermal properties of clathrate hydrates: a thermal conductivity study of tetrahydrofuran hydrate. *J. Phys. Chem. A* **1988**, *92*, 5006–5011.

(55) Koza, M. M.; Johnson, M. R.; Viennois, R.; Mutka, H.; Girard, L.; Ravot, D. Breakdown of phonon glass paradigm in La- and Ce-filled Fe₄Sb₁₂ skutterudites. *Nat. Mater.* **2008**, *7*, 805–810.

(56) Christensen, M.; Abrahamsen, A. B.; Christensen, N. B.; Juranyi, F.; Andersen, N. H.; Lefmann, K.; Andreasson, J.; Bahl, C. R. H.; Iversen, B. B. Avoided Crossing of Phonon Modes in Thermoelectric Materials. *Nat. Mater.* **2008**, *7*, 811–815.

(57) Dharma-Wardana, M. W. C. The thermal conductivity of the ice polymorphs and the ice clathrates. *J. Phys. Chem. A* **1983**, *87*, 4185–4190.

(58) Andersson, O.; Suga, H. Thermal Conductivity of the Ih and XI Phases of Ice. *Phys. Rev. B* **1994**, *50*, No. 6583.

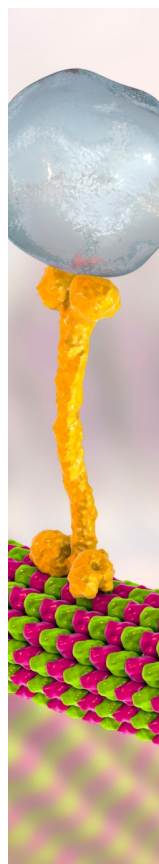
(59) Tse, J. S. Thermal Expansion of the Clathrate Hydrates of Ethylene Oxide and Tetrahydrofuran. *J. Phys. Colloq.* **1987**, *48*, C1-543–C1-549.

(60) Fortes, A. D. Accurate and precise lattice parameters of H₂O and D₂O ice Ih between 1.6 and 270 K from high-resolution time-of-flight neutron powder diffraction data. *Acta Crystallogr., Sect. B: Struct. Sci., Cryst. Eng. Mater.* **2018**, *B74*, 196–216.

(61) Leadbetter, A. J. The thermodynamic and vibrational properties of H₂O ice and D₂O ice. *Proc. R. Soc. London, Ser. A* **1965**, *287*, 403–425.

(62) Zakrzewski, M.; White, M. A. Derived thermodynamic properties of Dianin's inclusion compound, with and without guests. *J. Phys.: Condens. Matter* **1991**, *3*, 6703–6714.

(63) Slack, G. A. Thermal conductivity of ice. *Phys. Rev. B* **1980**, *22*, No. 3065.



CAS BIOFINDER DISCOVERY PLATFORM™

BRIDGE BIOLOGY AND CHEMISTRY FOR FASTER ANSWERS

Analyze target relationships,
compound effects, and disease
pathways

Explore the platform

CAS
A Division of the
American Chemical Society